CORA Cork Open Research Archive
Cartlann Taighde Oscailte Chorcaí

Title	Gap solitons in spatiotemporal photonic crystals
Authors	Biancalana, Fabio;Amann, Andreas;O'Reilly, Eoin P.
Publication date	2008
Original Citation	Biancalana, F., Amann, A. and O'Reilly, E. P. (2008) 'Gap solitons in spatiotemporal photonic crystals', Physical Review A, 77(1), 011801 (4pp). doi: 10.1103/PhysRevA.77.011801
Type of publication	Article (peer-reviewed)
Link to publisher's version	https://journals.aps.org/pra/abstract/10.1103/PhysRevA.77.011801 - 10.1103/PhysRevA.77.011801
Rights	© 2008, American Physical Society
Download date	2026-11-15 14:07:33
Item downloaded from	https://hdl.handle.net/10468/4542

UCC
University College Cork, Ireland
Coláiste na hOllscoile Corcaigh

Ground-state properties of a Tonks-Girardeau gas in a split trap

J. Goold* and Th. Busch
Department of Physics, National University of Ireland, UCC, Cork, Republic of Ireland
(Received 10 March 2008; published 2 June 2008)

We determine the exact many-body properties of a bosonic Tonks-Girardeau gas confined in a harmonic potential with a tunable δ-function barrier at the trap center. This is done by calculating the reduced single-particle density matrix, the pair-distribution function, and the momentum distribution of the gas as a function of barrier strength and particle number. With increasing barrier height we find that the ground-state occupation in a diagonal basis diverges from the $\sqrt{N}$ behavior that is expected for the case of a simple harmonic trap. In fact, the scaling of the occupation number depends on whether one has an even or odd number of particles. Since this quantity is a measure of the coherence of our sample we show how the odd-even effect manifests itself in both the momentum distribution of the Bose gas and interference fringe visibility during free temporal evolution.

DOI: 10.1103/PhysRevA.77.063601 PACS number(s): 03.75.Gg, 03.65.Ge, 37.10.De, 05.30.Jp

I. INTRODUCTION

The last two decades have seen considerable experimental and theoretical activity and progress in the area of cooling and trapping of neutral atoms. Several crowning achievements have been produced, including the realization of Bose-Einstein condensation [1], the creation of periodic arrays of single atoms [2] and the observation of superfluid phases in ultracold Fermi gases [3]. While research in this area is interesting from a fundamental point of view, ultracold atoms are also well-suited candidates to observe concepts and ideas in quantum information [4]. This is due to the fact that cold atomic samples are often well isolated from the environment, while being highly controllable at the same time, which is of paramount importance if one wants to create and work with fragile many-body states.

Two experimental advances have recently opened up the possibility to create and carry out experiments in strongly correlated quantum gases. The first one is due to optical lattices and atom chip traps, which can produce tightly confined potentials in selective directions of space. This allows one to limit the atom's degrees of freedom and thereby create effectively lower-dimensional systems [5,6]. Second, by the using Feshbach resonances or by tuning of the effective mass of particles moving in a periodic potential [5], the interparticle scattering length can be tuned to almost every value desired.

Combining these techniques has permitted the experimental realization of atomic gases in the so-called Tonks-Girardeau (TG) regime [5,6]. A TG gas is defined to be a one-dimensional, strongly correlated gas consisting of bosons that interact via a hardcore potential [7–9]. In the limit of pointlike interparticle interactions Girardeau found that such a model can be solved exactly by mapping it to an ideal, spinless fermionic system and he was the first to point out that a gas of strongly interacting bosons can thereby acquire certain fermionic properties [8]. More recently it was found that the above case is just a special case of a general mapping theorem between bosons and fermions in one dimension, which can interact with finite strength [10].

In order to find the many-particle solutions of a given geometry for the TG gas (or for noninteracting fermions) one must first know the exact single-particle eigenstates. However, since the list of exactly solvable single-particle problems in quantum mechanics is limited, there is also only a small number of many-particle problems in the Tonks limit that can be exactly solved. Recently an exact solution for the experimentally important harmonic potential was found [11,12] and here we will add another example to the list by describing a double well setting. As we aim for exact solvability, we have chosen the model of the δ-split trap [13], which comprises of a gas trapped in a harmonic oscillator potential split in the center by a pointlike repulsive potential. In a recent paper the case of a boson pair was rigorously analyzed in such a split trap for a range of interaction strengths up to and including the Tonks limit [14]. It has also been suggested in Ref. [15] that the δ-split trap could be used to excite dark soliton like structures in a Tonks-Girardeau gas.

Investigating the model of the δ-split potential can be justified in several ways. First it can be seen as an idealized model of a realistic double well situation where the height of the barrier is related to the area of a physical potential. Comparison of our results with recent numerical simulations show that the qualitative behavior we find here persists for reasonable and realistic values of finite sized splitting potentials [16–18]. Alternatively, a pointlike potential can be a good approximation to describe a strongly localized impurity within the bosonic gas [19,20].

Our main findings concern the coherence inherent in such samples. For the harmonically trapped case and in the thermodynamic limit it is known that the ground-state occupation scales as $\sqrt{N}$ [21]. However, for smaller samples it has been demonstrated that deviations from the $\sqrt{N}$ behavior exist and that macroscopic coherence effects can still be present [12]. Therefore in this work we put particular emphasis on examining the ground-state occupation fraction as we increase the height of the central δ-barrier.

The paper is organized as follows. In Sec. II we introduce the many-body Hamiltonian, describe the associated single-

*jgoold@phys.ucc.ie

 ©2008 The American Physical Society

particle eigenfunctions and eigenvalues and review the Fermi-Bose mapping theorem. Section III explores the physical many-body properties of our model by calculating the reduced single-particle density matrix (RSPDM) and the pair-correlation function. In Sec. IV we investigate the influence of the splitting strength on the ground-state occupation number and relate our results for this behavior to two experimentally realizable quantities, namely the momentum distribution and interference patterns. Finally, in Sec. V we make concluding remarks.

II. MODEL HAMILTONIAN AND THE FERMI-BOSE MAPPING THEOREM

A. System Hamiltonian

We consider a gas of N bosons trapped in a tight atomic waveguide. The waveguide restricts the dynamic of the gas strongly in the transversal directions, such that in the low-temperature limit we can restrict our model to the longitudinal direction only [22]. In this direction we then consider a δ-split harmonic potential such that at low linear density the many-particle Hamiltonian can be written as

$$\mathcal{H} = \sum_{n=1}^{N} \left(-\frac{\hbar^2}{2m}\frac{\partial^2}{\partial x_n^2} + \frac{1}{2}m\omega^2 x_n^2 + \kappa\delta(x_n) \right) + \sum_{i<j} V(|x_i - x_j|). \tag{1}$$

Here m is the mass of a single atom, ω the frequency of the harmonic potential, and κ is the strength of the pointlike splitting potential, which is located at $x=0$. Since we assume low densities, only elastic two-particle collision have to be considered and we can restrict the interaction potential to depend only on the relative distances. For bosonic systems at low temperatures the atomic interaction potential itself can be well approximated by a pointlike potential

$$V(|x_i - x_j|) = g_{1\mathrm{D}}\delta(|x_i - x_j|), \tag{2}$$

where $g_{1\mathrm{D}}$ is the one-dimensional (1D) coupling constant. This approximation is well justified for nonresonant situations and the only reminiscence of the exact potential is given by the three-dimensional s-wave scattering length $a_{3\mathrm{D}}$. For positive values of $a_{3\mathrm{D}}$ the interaction is repulsive and for negative values of $a_{3\mathrm{D}}$ it is attractive. Finally, the scattering length is related to the one-dimensional coupling constant via

$$g_{1\mathrm{D}} = \frac{4\hbar^2 a_{3\mathrm{D}}}{m a_\perp}(a_\perp - C a_{3\mathrm{D}})^{-1}, \tag{3}$$

where C is a constant of value $C=1.4603\cdots$ [22].

B. Eigenstates and eigenvalues of the δ-split trap

The single-particle eigenstates of the delta-split harmonic oscillator have recently been discussed in detail [23] and we will briefly review them here for completeness. To do this we rescale the single-particle part of the Hamiltonian (1)

$$h = -\frac{1}{2}\frac{\partial^2}{\partial \bar{x}^2} + \frac{1}{2}\bar{x}^2 + \bar{\kappa}\delta(\bar{x}), \tag{4}$$

where all lengths are in units of the ground-state size $a_0 = \sqrt{\hbar/m\omega}$ and all energies in terms of the oscillator energy $\hbar\omega$. This leads to a new scaled length given by $x=\bar{x}a_0$ and scaled barrier strength given by $\bar{\kappa}=(\hbar\omega a_0)^{-1}\kappa$. For notational simplicity we shall drop the overbars on all scaled quantities and acknowledge that we are, henceforth, dealing in the scaled units just described. All units used in figure plots in this paper are also in terms of these scaled units. The time-independent Schrödinger equation for this system now reads

$$h\psi_n(x) = E_n\psi_n(x). \tag{5}$$

It is immediately clear that the odd eigenfunctions of the simple harmonic oscillator are still good eigenfunctions for the δ-split oscillator, as they vanish at the exact position of the disturbance

$$\psi_n(x) = \mathcal{N}_n H_n(x) e^{-x^2/2}, \quad n = 1,3,5\ldots\ . \tag{6}$$

Here the $H_n(x)$ are the nth order Hermite polynomials and the $\mathcal{N}_n$ are the associated normalization constants. The corresponding energies are given by the eigenvalues of the odd parity states of the harmonic oscillator $E_n=(n+\frac{1}{2})$.

The even eigenstates of the simple harmonic oscillator, on the other hand, have an extremum at $x=0$. They are therefore strongly influenced by the splitting potential and can be found to be [23]

$$\psi_n(x) = \mathcal{N}_n e^{-x^2/2} U\left(\frac{1}{4} - \frac{E_n}{2}, \frac{1}{2}, x^2\right), \quad n = 0,2,4\ldots, \tag{7}$$

where the $U(a,b,z)$ are the Kummer functions [24]. The corresponding eigenenergies E_n are determined by the roots of the implicit relation

$$-\kappa = 2\frac{\Gamma\left(-\frac{E_n}{2}+\frac{3}{4}\right)}{\Gamma\left(-\frac{E_n}{2}+\frac{1}{4}\right)}. \tag{8}$$

Increasing the barrier height leads to an increase in the energy of the even eigenstates and in the limit of $\kappa=\infty$ each even eigenstate becomes energetically degenerate with the next higher lying odd eigenstate.

Since we know the single-particle eigenstates, we can build and solve the Slater determinant for a system of noninteracting fermions. Using the Fermi-Bose mapping theorem we can then calculate the many-particle bosonic wave function from the fermionic result.

C. The Fermi-Bose mapping theorem

While the original Fermi-Bose mapping theorem only related strongly interacting bosons to ideal fermions [8], it was recently found that the mapping idea can be applied to other systems as well [10]. Here we concentrate on the situation relevant to our system, i.e., the Tonks limit of infinite, pointlike repulsion ($g_{1\mathrm{D}}\to\infty$) between bosons. The main idea is that one can treat the interaction term in Eq. (1) by replacing it with the following boundary condition on the allowed bosonic wave function

$$\Psi_B = 0 \quad \text{if} \quad |x_i - x_j| = 0 \tag{9}$$

for $i \neq j$ and $1 \leq i \leq j \leq N$. As this is formally equivalent the Pauli exclusion principle, one can solve for the associated ideal fermionic wave function

$$\Psi_F(x_1, \ldots, x_N) = \frac{1}{\sqrt{N!}} \det_{n,j=1}^{N} [\psi_n(x_j)] \tag{10}$$

and calculate the bosonic solution from this by appropriate symmetrization

$$\Psi_B = A(x_1, \ldots, x_N)\Psi_F(x_1, x_2, \ldots, x_N), \tag{11}$$

where the unit antisymmetric function is given by [8]

$$A = \prod_{1 \leq i < j \leq N} \mathrm{sgn}(x_i - x_j). \tag{12}$$

As we are only interested in the ground state, this last step simplifies to

$$\Psi_B(x_1, \ldots, x_N) = |\Psi_F(x_1, \ldots, x_N)|. \tag{13}$$

III. MANY-BODY PROPERTIES

With the armory of the mapping theorem and the single-particle states available, we are now in a position to calculate various ground-state properties of the many-particle state as a function of increasing particle number as well as varying the strength of the central δ barrier.

A. Reduced single-particle density matrices

As laid out in the previous section, the Fermi-Bose mapping theorem allows for the calculation of the exact many-particle wave function. For the case of an infinitely strong barrier this was recently done analytically in Ref. [13]

$$\Psi_B = \frac{\tilde{C}}{\sqrt{N!}} 2^{N^2/8} \left[\prod_{j}^{N/2} e^{-x_j^2/4} |x_j| \right] \prod_{(j,k)=(1,j+1)}^{(N/2,N/2)} |x_j^2 - x_k^2|, \tag{14}$$

where $\tilde{C}$ is the normalization constant. Although this function fully characterizes the state of the system, other quantities can be more useful for obtaining characteristic properties of many-particle systems. We therefore proceed to calculate the reduced single-particle density matrix (RSPDM), from which expectation values of many important one-body physical observables such as the momentum distribution or the von Neumann entropy can easily be obtained.

For the bosonic gas, the RSPDM is defined as

$$\rho(x,x') = \int_{-\infty}^{+\infty} \Psi_B^*(x, x_2, \ldots, x_N) \times \Psi_B(x', x_2, \ldots, x_N) dx_2 \cdots dx_N, \tag{15}$$

and we choose its normalization to be given by $\int \rho(x,x)dx = N$. While for the simple harmonic oscillator this integral was solved analytically by Lapeyre *et al.* [25], we have to resort to a numerical evaluation for finite values of κ. Here we use an algorithm recently presented by Pezer and Buljan [26] that allows for effective calculation of Eq. (15) for large numbers of particles. In fact, our particle number is only limited by the numerical instabilities when calculating higher order Kummer functions.

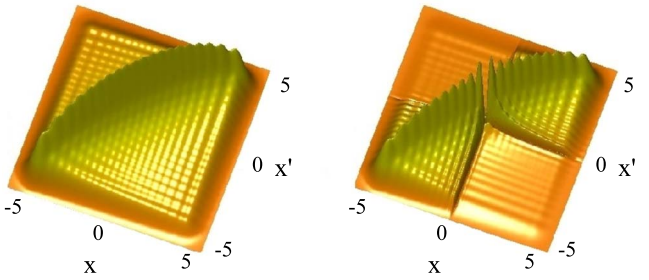


FIG. 1. (Color online) Reduced single-particle density matrices $\rho(x,x')$ for a Tonks gas of twenty particles for splitting strengths $\kappa=0$ (left) and $\kappa=20$ (right).

The RSPDM expresses self-correlation and one can view $\rho(x,x')$ as the probability that, having detected the particle at position x, a second measurement, immediately following the first, will find the particle at the point x'. Classically, $\rho(x,x')=\delta(x-x')$. The RSPDM for a twenty particle Tonks gas is shown in Fig. 1. In the unsplit case ($\kappa=0$) we see that most of the density is concentrated along the diagonal. Increasing κ introduces a gap around the position of the splitting potential $x=x'=0$, along with a reduction of density in the off diagonal regions. This is due to the suppression of tunneling from one side of the barrier to the other as the systems eigenstates become doubly degenerate in the $\kappa \to \infty$ limit.

The single-particle density can be calculated from the RSPDM by taking $x=x'$

$$\rho(x) = N \int_{-\infty}^{+\infty} |\Psi_B(x, x_2, \ldots, x_N)|^2 dx_2 \cdots dx_N, \tag{16}$$

and is therefore simply given by the diagonal of $\rho(x,x')$. In Fig. 2 we show this quantity for several different values if κ. In contrast to the self-correlations, one can see that the splitting effects the density only very locally. The results found in this case completely agree with the results presented in Ref. [13], where they were calculated in a different way by summing up the single-particle densities and symmetrizing.

To gain further understanding we next calculate the eigenvalues and eigenfunctions of the RSPDMs given by

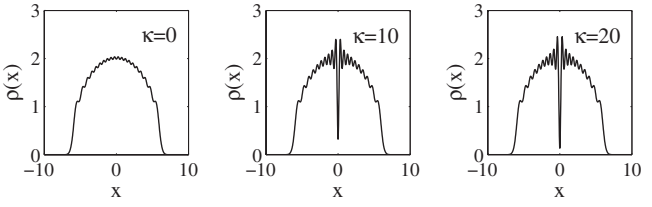


FIG. 2. Single-particle density for a Tonks gas of twenty particles for increasing barrier height.

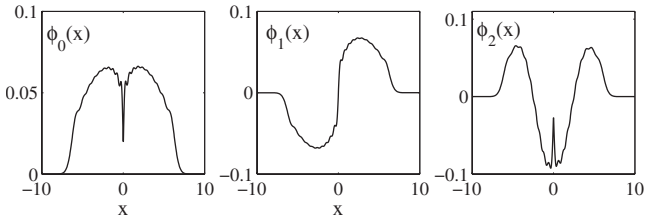


FIG. 3. The first three natural orbitals for a twenty particle Tonks gas in a δ-split trap with splitting strength $\kappa=20$.

$$\int_{-\infty}^{\infty} \rho(x,x')\phi_j(x')dx' = \lambda_j\phi_j(x). \tag{17}$$

The eigenfunctions $\phi_j(x)$ are known in theoretical chemistry as natural orbitals and their associated eigenvalues λ_j represent the occupation number of each orbital. The first three lowest energy natural orbitals for a twenty particle gas with a splitting potential of height $\kappa=20$ are displayed in Fig. 3. One can see the pointlike disturbance introduced by the δ function into the symmetric orbitals ϕ_0 and ϕ_2, while the antisymmetric ϕ_1 is unchanged from the $\kappa=0$ case (natural orbitals for the $\kappa=0$ case are displayed in Ref. [12]). These states and their occupation numbers will be used in Sec. IV to calculate the reciprocal momentum distributions and the ground-state occupations.

B. Pair distribution functions

The pair-distribution function $D(x_1,x_2)$, is a two-particle correlation function that describes the probability to measure two atoms at two given positions at the same time. It is defined in the following way:

$$D(x_1,x_2) = \mathcal{N}_D \int_{-\infty}^{+\infty} |\Psi_B(x_1,x_2,\ldots,x_N)|^2 dx_3 \cdots dx_N, \tag{18}$$

$$= \sum_{0\le n\le n'\le N-1}^{N-1} |\psi_n(x_1)\psi_{n'}(x_2) - \psi_n(x_2)\psi_{n'}(x_1)|^2, \tag{19}$$

where $\mathcal{N}_D=N(N-1)$. Since the terms with $n=n'$ in Eq. (19) vanish, and we can rewrite it in the following form:

$$D(x_1,x_2) = \rho(x_1)\rho(x_2) - |\Delta(x_1,x_2)|^2, \tag{20}$$

which is dependent only on the single-particle density and the correlation function $|\Delta(x_1,x_2)|$ defined by

$$|\Delta(x_1,x_2)| = \sum_{0\le n\le n'\le N-1}^{N-1} \psi_n^*(x_1)\psi_n(x_2). \tag{21}$$

The pair distribution functions for samples consisting of $N=5$, 10, and 30 particles and for barrier heights of $\kappa=0$, 1, and 10 are shown in Fig. 4. The first striking feature inherent to all situations is the absence of any probability along the diagonal, which is due to the impenetrable nature of the atoms. As the splitting strength is increased one observes the absence of probability for a joint measurement along the cross defined by the lines $x_1=0$ and $x_2=0$, which is again due to the central position of the δ splitting.

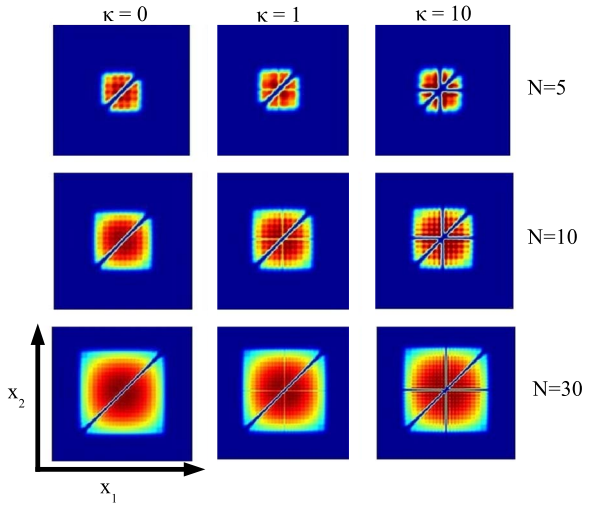


FIG. 4. (Color online) Pair distribution functions $D(x_1,x_2)$ for a Tonks gas of $N=5$, 10, and 30 particles in δ-split trap for splitting strengths $\kappa=0$, 1, and 10. In each plot the horizontal and vertical axes run from −10 to +10 in scaled units.

IV. GROUND-STATE OCCUPATION NUMBERS AND COHERENCE EFFECTS

The fraction of particles that are in the $\phi_0(x)$ orbital f is related to the largest eigenvalue λ_0 of the RSPDM by $f=\frac{\lambda_0}{N}$. Therefore, in analogy to the macroscopic occupation of a single eigenstate in a Bose-Einstein condensate, this orbital is sometimes referred to as the "BEC" state and the quantity λ_0 hence acts as a measure of the coherence in the system. Recently Forrester *et al.* have shown that, as one increases the particle number, λ_0/N tends toward $1/\sqrt{N}$ in the harmonically trapped case [21]. Here we will show how the introduction of a central barrier affects this $1/\sqrt{N}$ behavior in a dramatic way.

A. Occupation numbers

The fractional ground-state occupation λ_0/N is displayed in Fig. 5 as a function of particle number for different heights of the splitting potential. The dotted line corresponds to the unsplit trap ($\kappa=0$) and agrees with previously published results [21,27]. When increasing the magnitude of the splitting one notes a strikingly different behavior for the values of λ_0/N for odd and even particle numbers. For even particle numbers we find the coherence decreased as compared to the $\kappa=0$ case, whereas it is essentially unchanged when the particle number is odd. The effect becomes more pronounced as the splitting strength is increased and it damps out as the particle number is increased. This behavior is directly related to the magnitude of the RSPDM in the off-diagonal quadrants $\mathrm{sgn}(x)\neq\mathrm{sgn}(x')$ and therefore a clear signature of the coherence inherent in the system. To see this behavior manifest itself in an experimentally realizable quantity we will next calculate the momentum distribution as well as the visibility of interference fringes in the free evolution of the gas when released from the trap.

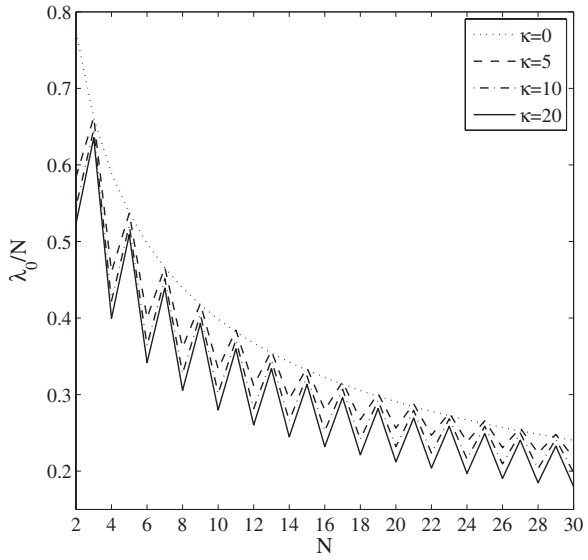


FIG. 5. Plot of the fractional ground-state occupation $f=\frac{\lambda_0}{N}$ versus particle number for a TG gas in a δ-split trap with increasing splitting strength.

B. Momentum distributions

For a harmonic trap the relationship between the momentum distribution and coherence properties of the TG was recently studied by Minguzzi and Gangardt [28]. The momentum distribution $n(k)$ can be calculated from the reduced single-particle density matrix

$$n(k) \equiv (2\pi)^{-1} \int_{-\infty}^{+\infty} \int_{-\infty}^{+\infty} \rho(x,x') e^{-ik(x-x')} dx dx', \quad (22)$$

and is normalized as $\int_{-\infty}^{+\infty} n(k)dk = N$. Equivalently it can be obtain by considering the eigenstates of $\rho(x,x')$. Using a discretized form for the quadrature then allows one to rewrite the integral equation as a linear algebraic equation

$$n(k) = \sum_i \lambda_i |\mu_i(k)|^2, \quad (23)$$

where $\mu_i(k)$ denotes the Fourier transform of the natural orbital $\phi_i(x)$,

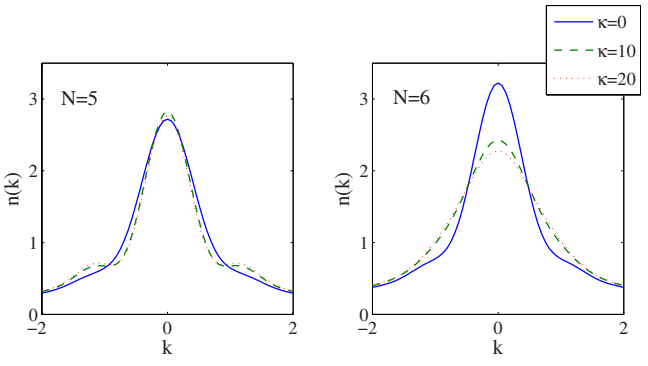


FIG. 6. (Color online) Central peaks of the momentum distributions $n(k)$ for TG gases consisting of $N=5$ (left) and $N=6$ (right) particles, for values of splitting strength $\kappa=0$, 10, and 20.

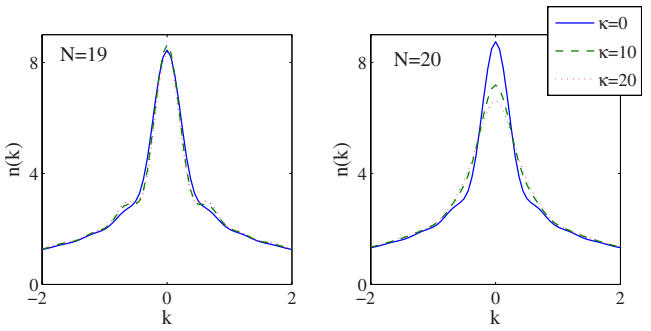


FIG. 7. (Color online) Central peak of the momentum distribution $n(k)$ for TG gases consisting of $N=19$ (left) and $N=20$ (right) particles, for values of splitting strength $\kappa=0$, 10, and 20.

$$\mu_i(k) = \frac{1}{\sqrt{2\pi}} \int_{-\infty}^{+\infty} \phi_i(x) e^{-ikx} dx. \quad (24)$$

The central peaks of the reciprocal momentum distribution for $N=5$ and $N=6$ particle samples are shown in Fig. 6 for different values of the splitting strengths. Figure 7 shows the same quantity for gases with $N=19$ and $N=20$ particles. While the states with odd particle numbers are clearly less affected by the barrier than the states with even particle number, one can see the emergence of bimodality at the neck of the peaks in the plots on the left hand side. It stems from the interference of particles on both sides of the splitting potential. For even particle number the introduction of the central splitting significantly broadens the momentum distribution lowers its peak. This is in agreement with analytical results we have found earlier for the special case of a two-particle Tonks molecule [14] and indicates a loss of coherence within the sample. The form of the momentum distributions displayed in Figs. 6 and 7 is determined by Eq. (23). In this equation λ_j acts as a weight on the contribution of the Fourier transform of an individual natural orbital. It is interesting to see which natural orbitals are responsible for the broadening of the distribution in the even particle case. In Fig. 8 the first six λ_j's are plotted as a function of κ for $N=19$ and $N=20$ particles. The difference between the odd and even samples can be clearly seen. In the $N=20$ case we see a degeneracy of consecutive eigenvalues occurring, this is due to the symmetry of having ten particles on the right of the

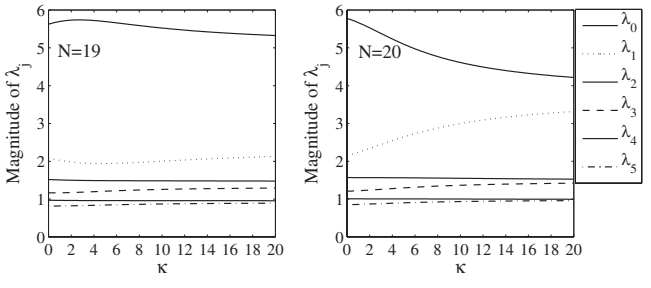


FIG. 8. Magnitude of the first six eigenvalues λ_j of $\rho(x,x')$ for $N=19$ and 20 particles as a function of the splitting strength κ. The lines of greatest magnitude represent λ_0 and decrease in the order $\lambda_0,\lambda_1,\lambda_2,\lambda_3,\lambda_4,\lambda_5$.

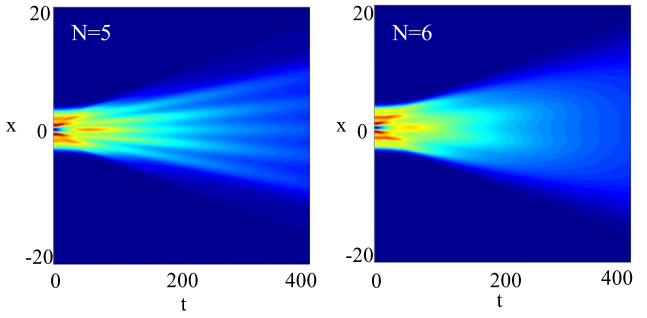


FIG. 9. (Color online) Free temporal evolution of the single-particle density $\rho(x,t)$ for a $N=5$ and 6 particle TG gas initially confined in a δ-split trap with $\kappa=100$.

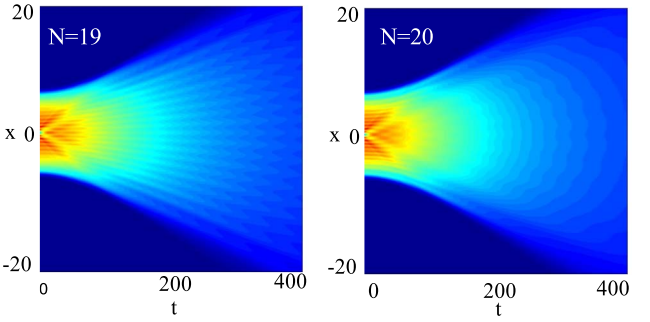


FIG. 10. (Color online) Free temporal evolution of the single-particle density $\rho(x,t)$ for a $N=19$ and 20 particle TG gas initially confined in a δ-split trap with $\kappa=100$.

barrier and ten on the left. The degeneracy explains why we have a noticeable change in the respective momentum distribution. In the $N=19$ case no such degeneracy occurs due to fact that one of the particles is spatially delocalized over both traps, this also explains the emergence of bimodality in the neck of the odd distributions. This behavior was found to be consistent for all particle numbers studied, up to 30 particles.

C. Interference fringes

The Fermi-Bose mapping theorem holds equally well for time-dependent ground-state wave functions and we will study the time evolution of the many-body quantum state after removal of the external potential. This situations is similar to one studied by Girardeau and Wright [11], who considered splitting and recombining a gas within an external trap. In our system splitting the sample is inherent in the Hamiltonian and we will pay special attention to effects stemming from different particle numbers. Starting off with the gas confined in the δ-split trap with large splitting amplitude, we look at the time evolution of the single-particle density $\rho(x,t)$ as both, the trap and the central splitting, are turned off and the gas undergoes free temporal evolution. During this both halves of the trap start overlapping and the densities for samples with $N=5$ and $N=6$ particles and with $N=19$ and $N=20$ particles are shown in Figs. 9 and 10, respectively. In both cases one can clearly see a more distinct interference pattern emerging for odd particle than for even particle samples, indicating that odd states carry larger coherence. In agreement with Fig. 5, the coherence effect is less pronounced at larger particle numbers but still clearly visible, as can be seen from Fig. 10.

It is well worth pointing out that as Figs. 9 and 10 show only density distributions, the results apply equally to a gas of spin polarized fermions. In this case, however, the interpretation of the variations of coherence with respect to particle number is straightforward, as the splitting introduces nonsmooth kinks in the single-particle wave function which create the Slater determinant.

V. CONCLUSIONS

Tonks gas has over the previous years shown to be an exciting and rich system to study new physics in a controlled way due to its analytic accessibility. Identifying and describing new potentials that take advantage of this is therefore of large importance. In the present work we have undertaken a thorough investigation of the many-body properties of the Tonks-Girardeau gas in a δ-split trap. We have calculated the RSPDM as well as the pair distribution function for various different splitting magnitudes and particle numbers and identified the basic physical behavior shown by the system.

From the RSPDMs we were able to study coherence properties of the gas by determining the behavior of the ground-state eigenvalue λ_0 as a function of particle number. Our results show that odd and even particle number samples obey different scaling laws, with the odd number samples remaining more coherent or less sensitive to the central splitting. The effect becomes less pronounced as one approaches larger particle numbers. To show how this effect manifest itself in different and experimentally observable quantities, we have studied the momentum distribution and interference experiments. For the momentum distributions we found that for odd particle numbers the sharp peak around momentum zero is relatively insensitive to the different strength of the splitting. For even particle numbers, however, the distributions are lowered and widened with increasing κ, demonstrating a loss in coherence. The simulations of the interference experiments for odd and even samples showed a larger visibility occurring for odd particle samples. This is in agreement with the other quantities that the odd number samples are more phase coherent.

ACKNOWLEDGMENTS

J.G. would like to thank D. O'Donoghue for valuable discussions. This project was supported by Science Foundation Ireland under Project No. 05/IN/I852.

[1] F. Dalfovo, S. Giorgini, L. P. Pitaevskii, and S. Stringari, Rev. Mod. Phys. **71**, 463 (1999).
[2] I. Bloch, J. Dalibard, and W. Zwerger, e-print arXiv:0704.3011 (2007).
[3] S. Giorgini, L. P. Pitaevskii, and S. Stringari, e-print arXiv:0706.3360 (2007).
[4] C. Monroe, Nature (London) **416**, 238 (2002).
[5] B. Paredes, A. Widera, V. Murg, O. Mandel, S. Fölling, I. Cirac, G. V. Shlyapnikov, T. W. Hänsch, and I. Bloch, Nature (London) **429**, 277 (2004).
[6] T. Kinoshita, T. Wenger, and D. S. Weiss, Science **305**, 1125 (2004).
[7] L. Tonks, Phys. Rev. **50**, 955 (1936).
[8] M. Girardeau, J. Math. Phys. **1**, 516 (1960).
[9] V. I. Yukalov and M. D. Girardeau, Laser Phys. Lett. **2**, 375 (2005).
[10] B. E. Granger and D. Blume, Phys. Rev. Lett. **92**, 133202 (2004).
[11] M. D. Girardeau and E. M. Wright, Phys. Rev. Lett. **84**, 5239 (2000).
[12] M. D. Girardeau, E. M. Wright, and J. M. Triscari, Phys. Rev. A **63**, 033601 (2001).
[13] Th. Busch and G. Huyet, J. Phys. B **36**, 2553 (2003).
[14] D. S. Murphy, J. F. McCann, J. Goold, and Th. Busch, Phys. Rev. A **76**, 053616 (2007).
[15] H. Buljan, O. Manela, R. Pezer, A. Vardi, and M. Segev, Phys. Rev. A **74**, 043610 (2006).
[16] D. S. Murphy, Ph.D. thesis, The Queen's University of Belfast, 2008.
[17] S. Zöllner, H.-D. Meyer, and P. Schmelcher, Phys. Rev. A **74**, 053612 (2006).
[18] S. Zöllner, H.-D. Meyer, and P. Schmelcher, Phys. Rev. A **74**, 063611 (2006).
[19] U. Gavish and Y. Castin, Phys. Rev. Lett. **95**, 020401 (2005).
[20] H. Fu and A. G. Rojo, Phys. Rev. A **74**, 013620 (2006).
[21] P. J. Forrester, N. E. Frankel, T. M. Garoni, and N. S. Witte, Phys. Rev. A **67**, 043607 (2003).
[22] M. Olshanii, Phys. Rev. Lett. **81**, 938 (1998).
[23] Th. Busch, B. G. Englert, K. Rzazewski, and M. Wilkens, Found. Phys. **28**, 549 (1998).
[24] *Handbook of Mathematical Functions*, edited by M. Abramowitz and I. Stegun (Dover, New York, 1972).
[25] G. J. Lapeyre, Jr., M. D. Girardeau, and E. M. Wright, Phys. Rev. A **66**, 023606 (2002).
[26] R. Pezer and H. Buljan, Phys. Rev. Lett. **98**, 240403 (2007).
[27] M. D. Girardeau, E. M. Wright, and J. M. Triscari, Phys. Rev. A **63**, 033601 (2001).
[28] A. Minguzzi and D. M. Gangardt, Phys. Rev. Lett. **94**, 240404 (2005).